Clayey Landslide Initiation and Acceleration Strongly Modulated by Soil Swelling

AUTHOR(S):

Schulz, William H.; Smith, Joel B.; Wang, Gonghui; Jiang, Yao; Roering, Joshua J.

CITATION:

Schulz, William H. ...[et al]. Clayey Landslide Initiation and Acceleration Strongly Modulated by Soil Swelling. Geophysical Research Letters 2018, 45(4): 1888-1896

ISSUE DATE:

2018-02-28

URL:

http://hdl.handle.net/2433/231097

AGU PUBLICATIONS

Geophysical Research Letters

RESEARCH LETTER
10.1002/2017GL076807

Key Points:
- Observed earthflow timing and speed correlated poorly with pore-water pressure
- Swelling of clayey soil increases landslide shear resistance concurrent with increasing pore-water pressure decreasing shear resistance
- The combined effects of lateral shear resistance from soil swelling and basal pore-water pressure can explain earthflow timing and mobility

Supporting Information:
- Supporting Information S1

Correspondence to:
W. H. Schulz,
wschulz@usgs.gov

Citation:
Schulz, W. H., Smith, J. B., Wang, G., Jiang, Y., & Roering, J. J. (2018). Clayey landslide initiation and acceleration strongly modulated by soil swelling. *Geophysical Research Letters*, *45*, 1888–1896. https://doi.org/10.1002/2017GL076807

Received 13 DEC 2017
Accepted 12 FEB 2018
Accepted article online 16 FEB 2018
Published online 26 FEB 2018

Clayey Landslide Initiation and Acceleration Strongly Modulated by Soil Swelling

William H. Schulz[1], Joel B. Smith[1], Gonghui Wang[2], Yao Jiang[2,3], and Joshua J. Roering[4]

[1]U.S. Geological Survey, Denver, CO, USA, [2]Disaster Prevention Research Institute, Kyoto University, Uji, Japan, [3]Now at Institute of Mountain Hazards and Environment, Chinese Academy of Sciences, Chengdu, China, [4]Department of Geological Sciences, University of Oregon, Eugene, OR, USA

Abstract Largely unknown mechanisms restrain motion of clay-rich, slow-moving landslides that are widespread worldwide and rarely accelerate catastrophically. We studied a clayey, slow-moving landslide typical of thousands in Northern California, USA, to decipher hydrologic-mechanical interactions that modulate landslide dynamics. Similar to some other studies, observed pore-water pressures correlated poorly with landslide reactivation and speed. In situ and laboratory measurements strongly suggested that variable pressure along the landslide's lateral shear boundaries resulting from seasonal soil expansion and contraction modulated its reactivation and speed. Slope-stability modeling suggested that the landslide's observed behavior could be predicted by including transient swell pressure as a resistance term, whereas modeling considering only transient hydrologic conditions predicted movement five to six months prior to when it was observed. All clayey soils swell to some degree; hence, our findings suggest that swell pressure likely modulates motion of many landslides and should be considered to improve forecasts of clayey landslide initiation and mobility.

1. Introduction

Landslides present significant hazards to human safety and the built environment, causing billions of dollars in damages (Spiker & Gori, 2003) and thousands of casualties (Kirschbaum et al., 2010; Petley, 2012) on an annual basis worldwide. Landslides also denude hillslopes and mobilize sediment that eventually impacts surface water bodies; in many regions, landslides are the primary agent of geomorphic change (Mackey & Roering, 2011; Roering et al., 2009; Schmidt & Montgomery, 1995; Simoni et al., 2013). The hazards that landslides present and their control on landscape change are largely dictated by the timing of their occurrence, their size, and the duration, speed, and total amount of their movement. However, although long studied, the ability to predict future landslide behavior remains challenging. Elevation of pore-water pressure is a primary cause of landslide failure and acceleration (e.g., Angeli et al., 1996; Bovis & Jones, 1992; Corominas et al., 2005; Fleming et al., 1988; Godt et al., 2008; Guerriero et al., 2014; Handwerger et al., 2013; Iverson, 2000, 2005; Iverson & Major, 1987; Keefer & Johnson, 1983; Lu & Likos, 2004; Malet et al., 2004; Montgomery et al., 1998; Schulz et al., 2009, 2012, 2017; Skempton et al., 1989; Terzaghi, 1950; van Asch, 2005; van Asch et al., 2007; Wang et al., 2010). As dictated by the oft-utilized Coulomb-Terzaghi failure criterion (e.g., Terzaghi et al., 1996), resistance to shear failure (τ) along landslide boundaries depends on cohesive stresses (c) and friction (ϕ) modulated by normal stress (σ) and pore-water pressure (p):

$$\tau = (\sigma - p)\ \tan\ \phi + c \tag{1}$$

Elevated pore-water pressure reduces normal stress to effective normal stress ($\sigma' = \sigma - p$), which reduces frictional resistance. Despite this understanding, identifying consistent and accurate pore-water pressure levels that instigate movement remains difficult for many landslides (e.g., Angeli et al., 1996; Gasparetto et al., 1996; Massey et al., 2013; Petley et al., 2005; Pyles et al., 1987; Shibasaki et al., 2016). Similarly, the observed speed of many landslides correlates poorly with pore-water pressure (e.g., Picarelli et al., 2004; Schulz et al., 2009; Shibasaki et al., 2016; van Asch, 2005; van Asch et al., 2007; Wienhöfer et al., 2010). Shear strength that increases with shearing rate has been proposed to explain the lack of acceleration to unbounded speeds for many slow-moving landslides (e.g., Angeli et al., 1996; Corominas et al., 2005; Iverson, 2000; Iverson & Major, 1987; Keefer & Johnson, 1983; Skempton et al., 1989; van Asch, 2005; van Asch et al., 2007; Vulliet & Hutter, 1988a, 1988b; Wang et al., 2010), but laboratory tests often reveal that gouge strengthening is negligible or too low to explain observations (e.g., Angeli et al., 1996; Baum & Johnson, 1993; Keefer & Johnson,

1983; Skempton, 1985; van Asch et al., 2007). We sought to improve understanding of controls on landslide initiation and speed by monitoring and testing materials from a persistent, slowly moving landslide (Two Towers; Figure S1) in Northern California, USA. We hypothesized that the landslide's activity strongly depended upon variable pressure along its lateral boundaries that resulted from seasonal soil swelling and shrinking.

2. Study Area

Thousands of landslides occur in Northern California that move persistently (including episodically on a seasonal basis) and slowly for many years (Handwerger et al., 2013; Keefer & Johnson, 1983; Kelsey, 1978; Mackey & Roering, 2011; Roering et al., 2009), resulting in morphology suggestive of flow. Thus, these landslides often are referred to as earthflows as described in the classification system of Hungr et al. (2001). Earthflows occur in many landscapes worldwide and locally dominate hillslope denudation and sediment transport (e.g., Bovis & Jones, 1992; Giordan et al., 2013; Keefer & Johnson, 1983; Kelsey, 1978; Mackey & Roering, 2011; Roering et al., 2009; Simoni et al., 2013). Although flow is implied by their name, ample evidence (e.g., Baum et al., 1993; Corominas et al., 2005; Fleming & Johnson, 1989; Keefer & Johnson, 1983; Schulz et al., 2009; Skempton et al., 1989) reveals that nearly all of their movement occurs by sliding along bounding shear zones, as with landslides, in general (e.g., Baum & Johnson, 1993; Skempton, 1985; Terzaghi, 1950). Earthflows typically occur in clayey granular material (soil), as do many other slowly moving landslides (e.g., Baum & Johnson, 1993; Terzaghi, 1950). The Two Towers landslide is typical of many earthflows in the region as indicated by its speed, composition, and failure mechanism being similar to those of more than 100 others that have been studied (Bennett et al., 2016; Handwerger et al., 2013, 2015; Iverson & Major, 1987; Keefer & Johnson, 1983; Kelsey, 1978; Mackey & Roering, 2011; Roering et al., 2009). The landslide occurs in Franciscan Complex mélange primarily comprising mudstone, sandstone, greenstone, chert, serpentinite, and schist that is tectonically sheared and weathered to mixtures of clay, silt, sand, and rock fragments (Handwerger et al., 2013; Kelsey, 1978; Mackey & Roering, 2011; Roering et al., 2009). Two Towers is ~250 m long and averages about 40 m wide and 7 m deep (Figures S1 to S3). The landslide's ground surface is inclined on average ~15° and is generally smooth and planar, suggesting a similarly smooth, planar base (Baum et al., 1993; Coe et al., 2009; Guerriero et al., 2014). The lateral boundaries of the landslide are approximately vertical to excavated depths of ~2 m, as are those of many other earthflows and slowly moving landslides (e.g., Fleming & Johnson, 1989; Guerriero et al., 2014; Kelsey, 1978; Schulz et al., 2009). Where exposed along its lateral boundaries, shear gouge is a few centimeters thick and heavily striated and slickensided. Remote-sensing studies (Bennett et al., 2016; Handwerger et al., 2013, 2015; Mackey & Roering, 2011; Roering et al., 2009; Roering et al., 2015) indicate that Two Towers and similar landslides in the region move primarily by shear translation at average speeds generally less than 1 m/year.

3. Methods

3.1. Field Monitoring

We made hourly measurements of rainfall, groundwater head, landslide movement, horizontal total stress, and vertical deformation of landslide material from 11 November 2014 to 22 July 2017. Rainfall was measured using a tipping-bucket gauge. Groundwater head was measured (0.01 m resolution, 0.03 m accuracy) at two depths each within the landslide head (3.66 and 6.07 m), middle (3.95 and 5.69 m), and toe (2.62 and 3.66 m) (Figures S1 to S3) using vibrating-wire piezometers placed within boreholes backfilled first with ~0.3 m of soil obtained during boring and then with bentonite granules to the ground surface. Horizontal total stress was measured at 1.83 m depth in the landslide center, and fluid stress also was measured at the same location (both with 0.01 kPa resolution, 0.07 kPa accuracy) to permit calculation of effective stress (σ'). The plate-shaped total stress sensor was installed within a slot oriented approximately normal to the landslide movement direction and which was made into the bottom of an excavated pit; the pit was subsequently backfilled. Landslide movement was measured using a 30.5 cm long biaxial tilt sensor (0.003 mm displacement resolution, long-term accuracy of 0.23 mm) installed within polyvinyl chloride-cased boreholes (i.e., a slope inclinometer). The slope inclinometer was used to attempt to identify the depth of the landslide base at each monitoring station and continuously measured landslide movement at the toe location. Potential vertical expansion and contraction of landslide material were measured using a borehole strain gauge (i.e., vertical deformation sensor;

0.04 mm resolution, 0.15 mm accuracy) with ends encased in cement such that it measured deformation over the depth interval 0.20–1.72 m upon installation. All sensors contained thermistors, and readings were temperature compensated, with the exception of the rain gauge.

3.2. Laboratory Testing

Samples for laboratory testing were obtained by hand from pits excavated to maximum depths of ~2 m. Water content, density, shrink-swell amount, swell pressure, torsional residual shear strength, particle-size distribution, and Atterberg limits were measured following respective ASTM standards (ASTM International, 2008). Mineralogy was determined by X-ray diffraction (Brown & Brindley, 1980; Eberl, 2003; Moore & Reynolds, 1997; Poppe et al., 2001). Some shear strength tests were performed using a specialized, large-scale ring-shear apparatus not covered by ASTM (DPRI-5; Sassa et al., 2004; Wang et al., 2010; Wang & Sassa, 2002). Additional details regarding strength testing are available in the supporting information.

4. Results

Table S1 provides properties of the landslide materials determined in the laboratory. Ring-shear tests indicated frictional resistance that was invariant with shearing rate within the tested range (0.0003 to 1 mm s^{-1}; Tables S2 and S3), as is commonly observed for slowly moving landslides (e.g., Baum & Johnson, 1993; Keefer & Johnson, 1983; Skempton, 1985). X-ray diffraction indicated that ~50–64% of the landslide material finer than 0.002 mm is composed of chlorite and illite/mica interstratified with smectite. Smectite is highly expansive, and swell pressure tests (Table S1) revealed that pressures of 118–310 kPa developed as water content increased from that measured in situ during April 2013 to saturation levels. Pressures of 320–695 kPa developed when specimens were initially air-dried and then saturated. For comparison, maximum normal stress (σ; equation (1)) calculated for the landslide base from laboratory and monitoring results (below) was 136 kPa. Although these swell pressures may seem extreme, they are typical of many expansive soils and similar to those measured in situ during other studies (Joshi & Katti, 1980; Brackley & Sanders, 1992). Swell potential generally correlates positively with liquid limit and clay content (e.g., Terzaghi et al., 1996), which is not apparent in Table S1. This lack of correlation was assumed to result from geological heterogeneity of the mélange in which the landslide was formed, and from specimens for the different tests for each generalized location (e.g., head, toe) being taken from distances as much as ~10 m apart.

Slope-inclinometer profiling indicated landslide thickness of 6.34, ~7.9, and 3.58 m for the head, middle, and toe locations, respectively. Considering the length of the inclinometer probes, shear gouge was less than 30.5 cm thick at the head location and less than 61 cm thick at the toe location; the inclinometer did not reveal nonmoving ground beneath the landslide at the middle location. Monitoring indicated that the upper ~1.7 m of the landslide experienced seasonal vertical expansion and contraction of 3 cm that correlated well with onset and cessation of the rainy season, respectively (Figure 1); however, expansion and contraction may have extended to greater depths. Significant seasonal changes in moisture content that cause expansion and contraction may have extended to depths of ~5 m, as implied by the water table dropping to this depth during the dry season (Figures S2 and S3). We observed contraction-induced opening of lateral bounding shear zones during the dry season (Figure S5) but total depths of opening were unknown (open to at least ~1 m depth where excavated). Pore-water pressures and horizontal total and effective stress were elevated during the rainy season and declined thereafter. Pressure head varied annually by ~3 m, on average, suggesting ~3 m of annual water table fluctuation. Horizontal effective stress increased by ~24 kPa during the rainy season; however, drying-induced soil shrinkage resulted in loss of soil contact with the sensor for approximately three to four months each year so actual effective stress varied by greater amounts. Consistent with our laboratory and monitoring observations, other monitoring studies reveal horizontal swell pressures of ~80–300 kPa upon wetting (Joshi & Katti, 1980; Brackley & Sanders, 1992). The region experienced extreme drought preceding and during the early part of our study that slowed most landslides (Bennett et al., 2016); we observed only minor movement (6–20 mm) during the spring and summer of 2015 and 2016. Prodigious rainfall occurred during late 2016 and early 2017 along with slide movement that was more typical (44 mm) for the region's earthflows (e.g., Handwerger et al., 2013, 2015); that motion continued to the end of our monitoring (22 July 2017). Landslide speed was similar to that observed for slow landslides throughout the region (Handwerger et al., 2013, 2015).

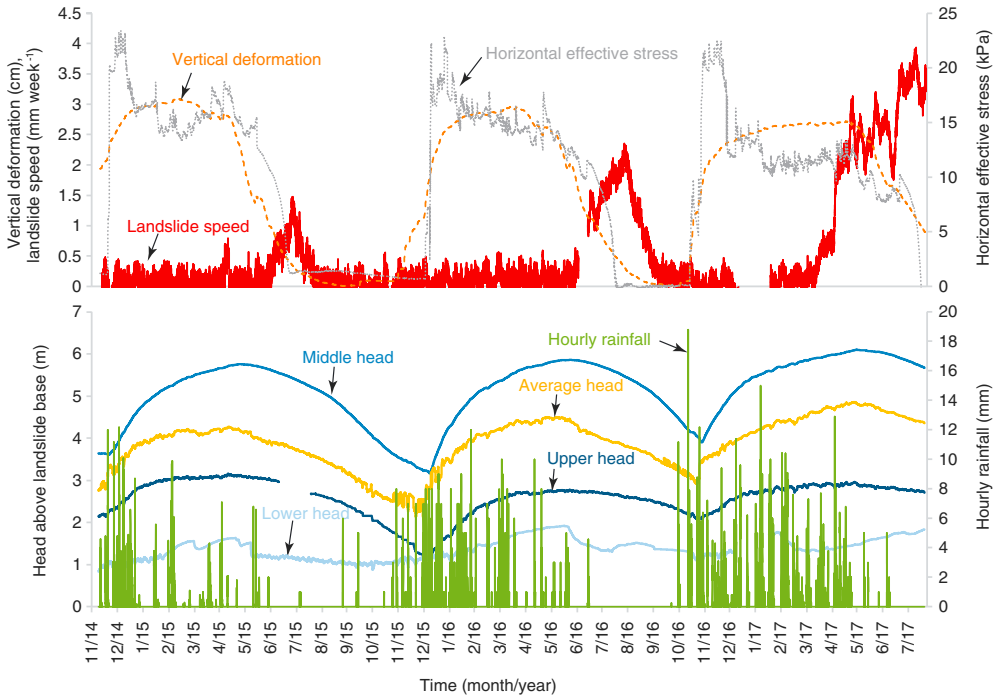

Figure 1. Results from continuous monitoring. Landslide speed is a five-day moving average. For clarity, records for one of the two piezometers at each monitoring location are displayed. Reductions in horizontal effective stress during the rainy season mostly resulted from increased head above the sensor; total horizontal stress was more nearly constant during the rainy season.

5. Discussion and Implications

As indicated by Figure 1 and in contrast with established theory regarding the importance of pore-water pressure on landslide stability (equation (1)), reactivated landslide motion did not occur at consistent pore-water pressures as has been reported previously (e.g., Angeli et al., 1996; Gasparetto et al., 1996; Massey et al., 2013; Petley et al., 2005; Pyles et al., 1987; Shibasaki et al., 2016), and movement generally occurred after peak pressures had passed. For example, average head above the landslide base calculated from our six piezometer records was 3.92, 4.34, and 4.62 when landslide movement initiated during 2015, 2016, and 2017, respectively, and was 3.57 and 3.43 when the landslide stopped moving during 2015 and 2016. Similarly, landslide speed often correlated poorly with pore-water pressure, with peak speed observed as pressure declined (Figure 1). Average head above the landslide base was 3.78, 3.85, and 4.41 when peak speeds were observed during 2015, 2016, and 2017, respectively. For evaluating landslide stability and rigorously testing the potential importance of pore-water pressure on landslide movement, equation (1) can be recast as the ratio of stresses resisting motion to those driving motion (often referenced as the factor of safety, F), with unity indicating incipient motion and values below unity indicating instability:

$$F(t) = \frac{\tan\varphi[(d\gamma_u + l\gamma_s)\cos\theta - p]}{(d\gamma_u + l\gamma_s)\sin\theta} \tag{2}$$

where d is the slope-normal depth of the water table; l is the slope-normal, water-saturated landslide thickness; θ is the angular inclination of the landslide base (assumed here to parallel the ground surface); and γ_u and γ_s are the weights of unit volumes of soil above and below the water table, respectively. Cohesion (c) in equation (1) is omitted here because it is assumed to be nil for fully developed shear gouge (i.e., in the residual strength condition) as exists at landslides that have moved farther than several centimeters to decimeters (e.g., Skempton, 1985; Terzaghi et al., 1996). Figure 2 shows $F(t)$ calculated using measured material properties, the average basal slope of 15°, an assumed average landslide thickness of 7 m (toe morphology suggested that our toe monitoring location was in an area of downslope thinning of the landslide),

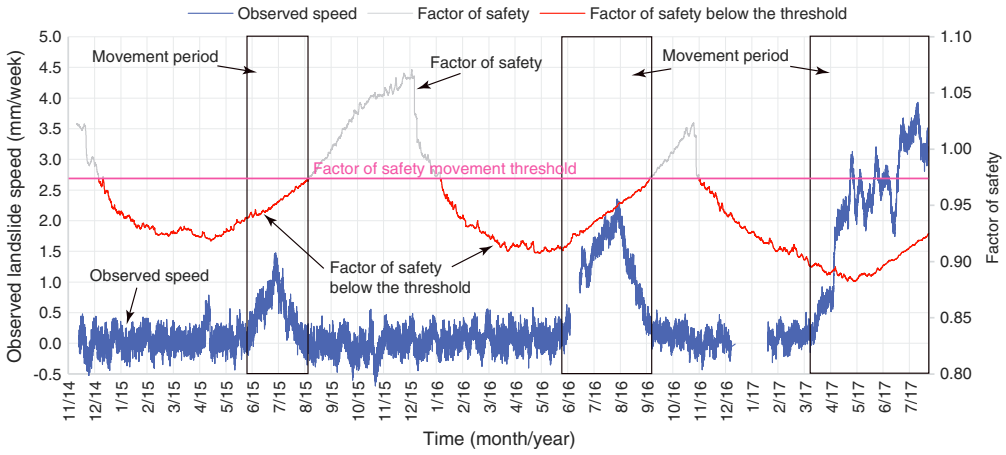

Figure 2. Results from typical landslide stability modeling. Factor of safety (*F*) was calculated using measured parameters and equation (2). The approximate threshold factor of safety was selected to capture all movement periods, and *F* is emphasized (with red color) when it is below the threshold; this threshold predicts movement for five to six months prior to when movement was observed.

and observed time series of *d*, *l*, and *p*, with these temporally dependent variables being averages from the six piezometers (values were linearly interpolated for missing records for deep head at the landslide head monitoring site 14 June 2015 to 22 July 2015 and shallow and deep head at the lower monitoring site 7 December 2016 to 18 January 2017). Emphasized in Figure 2 is the factor of safety range that implies landslide motion, which was selected by identifying the highest *F* (threshold *F*) at which motion was observed (0.974); perfect agreement between equation (2) results and observed motion at *F* below unity should not be expected because only one spatial dimension is considered by this use of equation (2). Although it captures all movement periods by definition, the threshold factor of safety poorly differentiates observed periods of motion from periods of stability (Figure 2). For example, it suggests that landslide movement should have commenced approximately five to six months prior to each movement episode and that landslide speed should have peaked approximately three months prior to when peak speeds were observed. Hence, as has been commonly observed and noted previously herein, mechanisms unrelated to pore-water pressure must have also been responsible for controlling the landslide's behavior.

Evaluation of Figure 1 indicates that pore-water pressures at the time of landslide reactivation were higher when soil swelling (as suggested by vertical deformation) was higher and vice versa; average head above the landslide base and vertical deformation at the time of the three reactivations were 3.92 and 1.0 cm, 4.34 and 1.8 cm, and 4.62 and 2.6 cm. Figure 1 also indicates that peak landslide speeds occurred as soil shrinkage was occurring and pore-water pressures were declining. We hypothesize that variable swell pressure along the lateral boundaries of the landslide served as a primary control on the landslide's reactivation and speed. Horizontal swell pressures are well known as being problematic in design and construction of foundation and retaining walls (Richards, 1985; Taylor & Smith, 1986; Basma et al., 1995; Terzaghi et al., 1996; Lu & Likos, 2004). Lateral earth pressure theory suggests that horizontal pressures are typically ~0.2–0.6 of vertical pressures in nonexpansive material (Terzaghi et al., 1996), whereas studies have shown that horizontal pressures may reach more than five times those of vertical pressures in expansive soils upon wetting (Richards, 1985). We observed annual horizontal effective stress variation approximately equivalent to the calculated vertical effective stress at the stress sensor location (Figure 1 and ~30 kPa, respectively); however, the lack of soil contact with the sensor during dry periods indicates that horizontal stress variations were higher than measured. Our laboratory tests revealed much greater inherent swell pressure in the material comprising the landslide body (Table S1). Swell pressure changing with moisture content may modulate frictional resistance along the landslide's lateral boundaries just as effective normal stress (σ') modulates frictional resistance along the landslide's basal boundary (equation (1)). As indicated by Figure 1, and as should be expected from infiltration of water at the ground surface, swell pressure (horizontal effective stress) increases immediately as moisture content rises (Aksu et al., 2015) and it does so at progressively greater

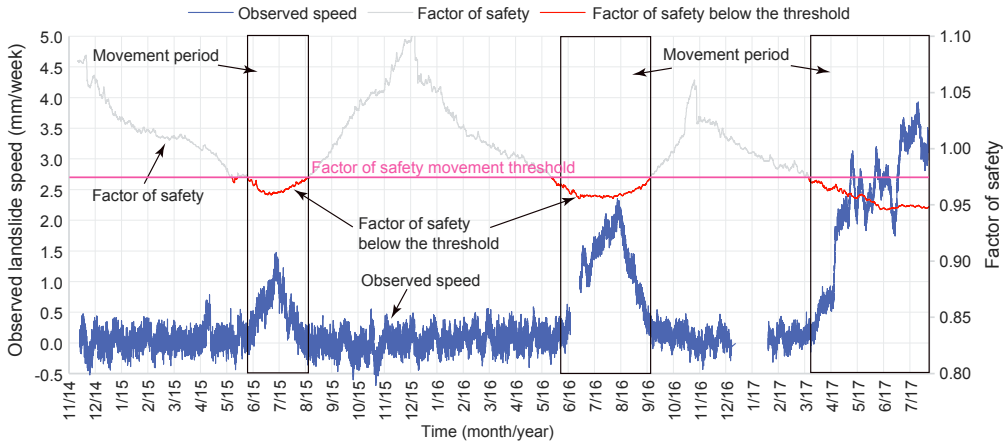

Figure 3. Results from landslide stability modeling considering resistance from variable swell pressure. Factor of safety (*F*) was calculated using measured parameters and equation (3). The approximate threshold factor of safety was selected to capture all movement periods, and *F* is emphasized (with red color) when it is below the threshold; this threshold predicts movement that strongly correlates with observed movement.

depths as wetting fronts move downward, resulting in increased swell (vertical deformation) of landslide material. During the rainy season, ongoing infiltration keeps soils above the water table in a swelled state, and these swelled soils behave essentially like caliper brakes on a wheel by increasing resistance to movement along the landslide's sides. With sufficient infiltration, pore-water pressures along the landslide's shear boundaries increase and reduce frictional resistance (equation (1)). If these pressures rise sufficiently high, as they may have during the winter and spring of 2017 (Figure 1), declining overall resistance to landsliding results in landslide acceleration. If pore-water pressures do not rise sufficiently high, landsliding might still occur during soil drying as swell pressures are consequently reduced, similar to releasing the brakes on the wheel. This is consistent with our observations during the spring-summer movement episodes of 2015 and 2016 (Figure 1). We test this conceptual model of swell-modulated landsliding below.

Three-dimensional modeling is required to fully account for swell and pore-water pressure effects along landslide lateral boundaries and concurrent pore-pressure effects along basal boundaries but would prove challenging, considering the variable depth and amount of swelling and uncertainty in proper consideration of changing lateral pressures, among other complications. However, our record of vertical deformation (Figure 1) reflects fluctuating soil volume as it seasonally swells and shrinks (the sensor averages effects of swelling over a great depth compared to the stress sensor), so we can use these measurements to estimate approximately the potential contribution of swell pressure to changing frictional resistance of the landslide's boundaries. Figure 3 shows results with the addition of the vertical deformation to the resistance term from equation (2) (numerator; cohesion [*c*] is again assumed to be nil):

$$F(t) = \frac{\tan\varphi[(d\gamma_u + l\gamma_s)\cos\theta - p + c_s S_n]}{(d\gamma_u + l\gamma_s)\sin\theta} \tag{3}$$

where S_n is swell pressure approximated by normalizing the vertical deformation time series by the maximum observed amount (3 cm) and c_s is a constant determined through iteration. Using the same factor of safety threshold of 0.974 used for Figure 2, the best fit c_s was 9.1, suggesting that swelling contributed as much as 3.1 kPa of resistance to landslide motion, or ~8–9% of the total resistance; the landslide lateral boundaries account for ~26% of the overall boundary. As indicated by Figure 3, including resistance from soil swelling along the landslide's lateral boundaries resulted in nearly perfect agreement between observed and modeled timing of landslide motion. Additionally, landslide speeds generally correlated well with the factor of safety, with peak speeds occurring during lowest *F*, and speeds for given movement periods being higher when *F* was lower. The addition of swell resistance results in much smaller factor of safety declines than expected from pore-pressure change (Figure 2), suggesting that swell-induced increased resistance restrains landslide acceleration and may help to prevent catastrophic landsliding. We conclude that swell pressure

strongly modulated mobility of the landslide we studied and likely had similar influence on other landslides for which Two Towers is a typical representative.

As with many landslides (e.g., Angeli et al., 1996; Bovis & Jones, 1992; Gasparetto et al., 1996; Handwerger et al., 2013; Petley et al., 2005; Picarelli et al., 2004; Pyles et al., 1987; Shibasaki et al., 2016; van Asch, 2005; van Asch et al., 2007; Wienhöfer et al., 2010), behavior of the Two Towers landslide could not be well predicted from pore-pressure variation alone. Angeli et al. (1996) observed higher pore-water pressure at landslide initiation than at cessation, similar to our observations, and concluded that this was due to shear strength of the landslide they studied increasing during suspension of landsliding. Our monitoring revealed inconsistent pore-water pressures at landslide reactivation, and our laboratory tests failed to reveal strength recovery between tests (although testing only indirectly explored recovery), so this mechanism was likely unimportant at Two Towers. Accelerated shear-induced dilation may cause declining pore-water pressure and increased shear resistance during accelerated landslide motion, which may restrain some landslides (e.g., Iverson, 2005; Schulz et al., 2009), but this mechanism is not supported by our monitoring or testing results. Some studies (van Asch, 2005; van Asch et al., 2007) concluded that landslide speed differences at identical pore-water pressures could be due to extension and compression of moving landslide material and related changes to localized pore-water pressures and material properties. Deformation of landslide material as it overrides wavy basal boundaries and consequent changes in pore-water pressure also likely contribute resistance to motion of many landslides (Baum & Johnson, 1993; Keefer & Johnson, 1983; Mizuno, 1989). Although often proposed, but rarely demonstrated (e.g., Angeli et al., 1996; Baum & Johnson, 1993; Iverson, 2000; Iverson & Major, 1987; Keefer & Johnson, 1983; Skempton, 1985; van Asch et al., 2007; Vulliet & Hutter, 1988a, 1988b; Wang et al., 2010), strengthening of boundary shear gouge at increased shear rates was unimportant at Two Towers, based on our laboratory results. Our results strongly suggest that variable swell pressure modulated the landslide's timing and speed and could account for the inconsistent pore-water pressure observed during its reactivation and movement. We therefore expect that variable swell pressure at other clayey landslides may at least partly account for similar poor correlations between landslide activity and pore-water pressure. Increased resistance from swelling apparently caused Two Towers to move more slowly than it probably would in the absence of swelling (Figures 2 and 3), and we conclude that this mechanism may also slow other clayey landslides.

Clay soils susceptible to significant swelling occupy ~20% of the land surface of the United States, whereas clay minerals compose approximately two thirds of argillaceous sediments that form ~60% of stratigraphy worldwide (Taylor & Smith, 1986). Essentially, all clay is expansive to some degree upon wetting (Mitchell & Soga, 2005; Terzaghi et al., 1996), with pressures for some clay mixtures reaching nearly 10 MPa (Basma et al., 1995). Therefore, we conclude that soil swelling may partly determine timing and speed of many landslides, with the degree to which it does so determined by multiple factors. Swell pressure may be a critical behavioral control for landslides such as Two Towers with its relatively high content of expansive clay, whereas swell pressure would have negligible effect in materials with low expansion potential. Landslide geometry should largely determine potential consequences of variable swell pressure; swelling should have reduced effect as landslide lateral boundaries flatten from vertical, as the ratio of lateral boundary dimensions relative to basal boundary (i.e., subparallel to the ground surface) dimensions decreases, and as the proportion of swell pressure variation decreases relative to pore-water pressure variation. Additionally, soil expansion and contraction may modify hydraulic (Aksu et al., 2015; Lu & Likos, 2004) and strength properties (Lu & Likos, 2004; Terzaghi et al., 1996). Hence, the effects of swelling are complex, necessitating further study. Our findings strongly suggest that swell pressures can modulate landslide timing and speed and may reduce the potential for catastrophic landslide motion. Swell pressures therefore should be considered for evaluating landslide hazards and the impacts of landslides on the landscape.

Acknowledgments
This study benefited from the support provided by Toshitaka Kamai, Amelia Deuell, Ryan Reeves, Alexander Handwerger, Ludwig Keller, CAMET Research, Inc., Cooper Testing Labs, Inc., Calvin and Wendy Stewart, Jim and TinaMarie Schaafsma, and Austin and Logan Scott. The study was funded by the U.S. Geological Survey Landslide Hazards Program; the Center Research for 2017 Collaborative Research of the Disaster Prevention Research Institute, Kyoto University (28A-04) (G. W. and Y. J.); and NASA grant NNX15AR59G (J. J. R., W. H. S., and J. B. S.). Any use of trade, firm, or product names is for descriptive purposes only and does not imply endorsement by the U.S. Government. Data that support this study are available in Schulz et al. (2018).

References

Aksu, I., Bazilevskaya, E., & Karpyn, Z. T. (2015). Swelling of clay minerals in unconsolidated porous media and its impact on permeability. *Geo Res J*, *7*, 1–13.

Angeli, M.-G., Gasparetto, P., Menotti, R. M., Pasuto, A., & Silvano, S. (1996). A visco-plastic model for slope analysis applied to a mudslide in Cortina d-Ampezzo, Italy. *Quarterly Journal of Engineering Geology*, *29*(3), 233–240. https://doi.org/10.1144/GSL.QJEGH.1996.029.P3.06

ASTM International (2008). *Annual book of ASTM Standards* (Vol. 04.08). West Conshohocken, PA: ASTM International.

Basma, A. A., Al-Homoud, A. S., & Husien (Malkawi), A. (1995). Laboratory assessment of swelling pressure of expansive soils. *Applied Clay Science*, *9*(5), 355–368. https://doi.org/10.1016/0169-1317(94)00032-L

Baum, R. L., Fleming, R. W., & Johnson, A. M. (1993). *Kinematics of the Aspen Grove Landslide, Ephraim Canyon, Central Utah, U.S. Geological Survey bulletin 1842-F*. Reston, VA: U.S. Geological Survey.

Baum, R. L., & Johnson, A. M. (1993). *Steady movement of landslides in fine-grained soils—A model for sliding over an irregular slip surface, U.S. Geological Survey bulletin 1842-D*. Reston, VA: U.S. Geological Survey.

Bennett, G. L., Roering, J. J., Mackey, B. H., Handwerger, A. L., Schmidt, D. A., & Guillod, B. P. (2016). Historic drought puts the brakes on earthflows in Northern California. *Geophysical Research Letters*, *43*, 5725–5731. https://doi.org/10.1002/2016GL068378

Bovis, M. J., & Jones, P. (1992). Holocene history of earthflow mass movements in south-central British Columbia: The influence of hydroclimatic changes. *Canadian Journal of Earth Sciences*, *29*(8), 1746–1755. https://doi.org/10.1139/e92-137

Brackley, I. J. A., & Sanders, P. J. (1992). In situ measurement of total natural horizontal stresses in an expansive clay. *Geotechnique*, *42*(3), 443–451. https://doi.org/10.1680/geot.1992.42.3.443

Brown, G., & Brindley, G. W. (Eds.) (1980). *Crystal structures of clay minerals and their X-ray identification* (Vol. 5). London: Mineralogical Society.

Coe, J. A., McKenna, J. P., Godt, J. W., & Baum, R. L. (2009). Basal-topographic control of stationary ponds on a continuously moving landslide. *Earth Surface Processes and Landforms*, *34*(2), 264–279. https://doi.org/10.1002/esp.1721

Corominas, J., Moya, J., Ledesma, A., Lloret, A., & Gili, J. (2005). Prediction of ground displacement velocities from groundwater level changes at the Vallcebre landslide (eastern Pyrenees, Spain). *Landslides*, *2*(2), 83–96. https://doi.org/10.1007/s10346-005-0049-1

Eberl, D. D. (2003). *User's guide to Rockjock—A program for determining quantitative mineralogy from X-ray diffraction Data, U.S. Geological Survey open file report 03–78*. Reston, VA: U.S. Geological Survey.

Fleming, R. W., & Johnson, A. M. (1989). Structures associated with strike-slip faults that bound landslide elements. *Engineering Geology*, *27*(1-4), 39–114. https://doi.org/10.1016/0013-7952(89)90031-8

Fleming, R. W., Schuster, R. L., & Johnson, R. B. (1988). *Physical properties and mode of failure of the Manti landslide, Utah, U.S. Geological Survey Professional Paper 1311 27–41*. Reston, VA: U.S. Geological Survey.

Gasparetto, P., Mosselman, M., & van Asch, T. W. J. (1996). The mobility of the Alverà landslide (Cortina d' Ampezzo, Italy). *Geomorphology*, *15*(3-4), 327–335. https://doi.org/10.1016/0169-555X(95)00078-J

Giordan, D., Allasia, P., Manconi, A., Baldo, M., Satangelo, M., Cardinali, M., et al. (2013). Morphological and kinematic evolution of a large earthflow: The Montaguto landslide, southern Italy. *Geomorphology*, *187*, 61–79. https://doi.org/10.1016/j.geomorph.2012.12.035

Godt, J. W., Baum, R. L., Savage, W. Z., Salciarini, D., Schulz, W. H., & Harp, E. L. (2008). Transient deterministic shallow landslide modeling: Requirements for susceptibility and hazard assessments in a GIS framework. *Engineering Geology*, *102*(3-4), 214–226. https://doi.org/10.1016/j.enggeo.2008.03.019

Guerriero, L., Coe, J. A., Revellino, P., Grelle, G., Pinto, F., & Guadagno, F. M. (2014). Influence of slip-surface geometry on earth-flow deformation, Montaguto earth flow, southern Italy. *Geomorphology*, *219*, 285–305. https://doi.org/10.1016/j.geomorph.2014.04.039

Handwerger, A. L., Roering, J. J., & Schmidt, D. A. (2013). Controls on the seasonal deformation of slow-moving landslides. *Earth and Planetary Science Letters*, *377*, 239–247.

Handwerger, A. L., Roering, J. J., Schmidt, D. A., & Rempel, A. W. (2015). Kinematics of earthflows in the Northern California coast ranges using satellite interferometry. *Geomorphology*, *246*, 321–333. https://doi.org/10.1016/j.geomorph.2015.06.003

Hungr, O., Evans, S. G., Bovis, M. J., & Hutchinson, J. N. (2001). A review of the classification of landslides of the flow type. *Environmental & Engineering Geoscience*, *VII*, 221–238.

Iverson, R. M. (2000). Landslide triggering by rain infiltration. *Water Resources Research*, *36*(7), 1897–1910. https://doi.org/10.1029/2000WR900090

Iverson, R. M. (2005). Regulation of landslide motion by dilatancy and pore pressure feedback. *Journal of Geophysical Research*, *110*, F02015. https://doi.org/10.1029/2004JF000268

Iverson, R. M., & Major, J. J. (1987). Rainfall, ground-water flow, and seasonal movement at Minor Creek landslide, northwestern California: Physical interpretation of empirical relations. *GSA Bulletin*, *99*(4), 579–594. https://doi.org/10.1130/0016-7606(1987)99%3C579:RGFASM%3E2.0.CO;2

Joshi, R. P., & Katti, R. K. (1980). *Lateral pressure development under surcharges*. Paper presented at 4th International Conference on Expansive Soils, Denver, CO.

Keefer, D. K., & Johnson, A. M. (1983). *Earth flows: Morphology, mobilization, and movement, U.S. Geological Survey professional paper 1264*. Reston, VA: U.S. Geological Survey.

Kelsey, H. M. (1978). Earthflows in Franciscan mélange, van Duzen River basin, California. *Geology*, *6*(6), 361–364. https://doi.org/10.1130/0091-7613(1978)6%3C361:EIFMVD%3E2.0.CO;2

Kirschbaum, D. B., Adler, R., Hong, Y., Hill, S., & Lerner-Lam, A. (2010). A global landslide catalog for hazard applications: Method, results, and limitations. *Natural Hazards*, *52*(3), 561–575. https://doi.org/10.1007/s11069-009-9401-4

Lu, N., & Likos, W. J. (2004). *Unsaturated Soil Mechanics*. NJ: John Wiley & Sons.

Mackey, B. H., & Roering, J. J. (2011). Sediment yield, spatial characteristics, and the long-term evolution of active earthflows determined from airborne LiDAR and historical aerial photographs, Eel River, California. *Geological Society of America Bulletin*, *123*(7-8), 1560–1576. https://doi.org/10.1130/B30306.1

Malet, J.-P., Maquaire, O., Locat, J., & Remaitre, A. (2004). Assessing debris flow hazards associated with slow moving landslides: Methodology and numerical analyses. *Landslides*, *1*(1), 83–90. https://doi.org/10.1007/s10346-003-0005-x

Massey, C. I., Petley, D. N., & McSaveney, M. J. (2013). Patterns of movement in reactivated landslides. *Engineering Geology*, *159*, 1–19. https://doi.org/10.1016/j.enggeo.2013.03.011

Mitchell, J. K., & Soga, K. (2005). *Soil composition and engineering properties. Fundamentals of soil behavior*. NJ: John Wiley & Sons.

Mizuno, K. (1989). *Landsliding of clayey slopes with a wavy slip surface model and its application: Science Reports of the Institute of Geosciences* (Vol. 10, pp. 87–151). Tsukuba: University of Tsukuba.

Montgomery, D. R., Sullivan, K., & Greenberg, H. M. (1998). Regional test of a model for shallow landsliding. *Hydrological Processes*, *12*(6), 943–955. https://doi.org/10.1002/(SICI)1099-1085(199805)12:6%3C943::AID-HYP664%3E3.0.CO;2-Z

Moore, D. M., & Reynolds, R. C. (1997). *X-ray diffraction and the identification and analysis of clay minerals*. Oxford: Oxford University Press.

Petley, D. (2012). Global patterns of loss of life from landslides. *Geology*, *40*(10), 927–930. https://doi.org/10.1130/G33217.1

Petley, D. N., Mantovani, F., Bulmer, M. H., & Zannoni, A. (2005). The use of surface monitoring data for the interpretation of landslide movement patterns. *Geomorphology*, *66*(1-4), 133–147. https://doi.org/10.1016/j.geomorph.2004.09.011

Picarelli, L., Urciuoli, G., & Russo, C. (2004). Effect of groundwater regime on the behaviour of clayey slopes. *Canadian Geotechnical Journal*, *41*(3), 467–484. https://doi.org/10.1139/t04-009

Poppe, L. J., Paskevich, V. F., Hathaway, J. C., & Blackwood, D. S. (2001). *A laboratory manual for X-ray powder diffraction, U.S. Geological Survey open-file report 01–041*. Reston, VA: U.S. Geological Survey.

Pyles, M. R., Mills, K., & Saunders, G. (1987). Mechanics and stability of the Lookout Creek earth flow. *Bulletin of the Association of Engineering Geologists*, *XXIV*(2), 267–280.

Richards, B. G. (1985). Pressures on a retaining wall by an expansive clay. In *Golden Jubilee of the International Society for Soil Mechanics and Foundation Engineering: Commemorative Volume* (pp. 241–246). Barton, A.C.T.: Institution of Engineers, Australia.

Roering, J. J., Mackey, B. H., Handwerger, A. L., Booth, A. M., Schmidt, D. A., Bennett, G. L., & Cerovski-Darriau, C. (2015). Beyond the angle of repose: A review and synthesis of landslide processes in response to rapid uplift, Eel River, Northern California. *Geomorphology*, *236*, 109–131. https://doi.org/10.1016/j.geomorph.2015.02.013

Roering, J. J., Stimely, L. L., Mackey, B. H., & Schmidt, D. A. (2009). Using DInSAR, airborne LiDAR, and archival air photos to quantify landsliding and sediment transport. *Geophysical Research Letters*, *36*, L19402. https://doi.org/10.1029/2009GL040374

Sassa, K., Fukuoka, H., Wang, G., & Ishikawa, N. (2004). Undrained dynamic-loading ring-shear apparatus and its application to landslide dynamics. *Landslides*, *1*(1), 7–19. https://doi.org/10.1007/s10346-003-0004-y

Schmidt, K. M., & Montgomery, D. R. (1995). Limits to relief. *Science*, *270*(5236), 617–620. https://doi.org/10.1126/science.270.5236.617

Schulz, W. H., Coe, J. A., Ricci, P. P., Smoczyk, G. M., Shurtleff, B. L., & Panosky, J. (2017). Landslide kinematics and their potential controls from hourly to decadal timescales: Insights from integrating ground-based InSAR measurements with structural maps and long-term monitoring data. *Geomorphology*, *285*, 121–136. https://doi.org/10.1016/j.geomorph.2017.02.011

Schulz, W. H., Galloway, S. L., & Higgins, J. D. (2012). Evidence for earthquake triggering of large landslides in coastal Oregon, USA. *Geomorphology*, *141-142*, 88–98. https://doi.org/10.1016/j.geomorph.2011.12.026

Schulz, W. H., McKenna, J. P., Biavati, G., & Kibler, J. D. (2009). Relations between hydrology and velocity of a continuously moving landslide—Evidence of pore-pressure feedback regulating landslide motion? *Landslides*, *6*(3), 181–190. https://doi.org/10.1007/s10346-009-0157-4

Schulz, W. H., Smith, J. B., Wang, G., Jiang, Y., Deuell, A., Reeves, R. R., et al. (2018). *Data from in-situ landslide monitoring*. Trinity County, CA: U. S. Geological Survey data release. https://doi.org/10.5066/F7GF0SFS

Shibasaki, T., Matsuura, S., & Okamoto, T. (2016). Experimental evidence for shallow, slow-moving landslides activated by a decrease in ground temperature. *Geophysical Research Letters*, *43*, 6975–6984. https://doi.org/10.1002/2016GL069604

Simoni, A., Ponza, A., Picotti, V., Berti, M., & Dinelli, E. (2013). Earthflow sediment production and Holocene sediment record in a large Apennine catchment. *Geomorphology*, *188*, 42–53. https://doi.org/10.1016/j.geomorph.2012.12.006

Skempton, A. W. (1985). Residual strength of clays in landslides, folded strata, and the laboratory. *Geotechnique*, *35*(1), 3–18. https://doi.org/10.1680/geot.1985.35.1.3

Skempton, A. W., Leadbeater, A. D., & Chandler, R. J. (1989). The mam tor landslide, north Derbyshire. *Philosophical Transactions of the Royal Society of London. Series A*, *329*(1607), 503–547. https://doi.org/10.1098/rsta.1989.0088

Spiker, E. C., & Gori, P. L. (2003). *National landslide hazards mitigation strategy—A framework for loss reduction, U.S. Geological Survey circular 1244*. Reston, VA: U.S. Geological Survey.

Taylor, R. K., & Smith, T. J. (1986). The engineering geology of clay minerals: Swelling, shrinking and mudrock breakdown. *Clay Minerals*, *21*(3), 235–260. https://doi.org/10.1180/claymin.1986.021.3.01

Terzaghi, K. (1950). Mechanism of landslides. In S. Paige (Ed.), *Application of geology to engineering practice (Berkey volume)*. New York: Geological Society of America.

Terzaghi, K., Peck, R. B., & Mesri, G. (1996). *Soil mechanics in engineering practice*. New York: John Wiley & Sons.

van Asch, T. W. J. (2005). Modelling the hysteresis in the velocity pattern of slow-moving earth flows: The role of excess pore pressure. *Earth Surface Processes and Landforms*, *30*(4), 403–411. https://doi.org/10.1002/esp.1147

van Asch, T. W. J., Van Beek, L. P. H., & Bogaard, T. A. (2007). Problems in predicting the mobility of slow-moving landslides. *Engineering Geology*, *91*(1), 46–55. https://doi.org/10.1016/j.enggeo.2006.12.012

Vulliet, L., & Hutter, K. (1988a). Viscous-type sliding laws for landslides. *Canadian Geotechnical Journal*, *25*(3), 467–477. https://doi.org/10.1139/t88-052

Vulliet, L., & Hutter, K. (1988b). Continuum model for natural slopes in slow movement. *Geotechnique*, *38*(2), 199–217. https://doi.org/10.1680/geot.1988.38.2.199

Wang, G., & Sassa, K. (2002). Post-failure mobility of saturated sands in undrained load-controlled ring shear tests. *Canadian Geotechnical Journal*, *39*(4), 821–837. https://doi.org/10.1139/t02-032

Wang, G., Suemine, A., & Schulz, W. H. (2010). Shear-rate-dependent strength control on the dynamics of rainfall-triggered landslides, Tokushima prefecture, Japan. *Earth Surface Processes and Landforms*, *35*, 407–416.

Wienhöfer, J., Lindenmaier, F., & Zehe, E. (2010). Challenges in understanding the hydrologic controls on the mobility of slow-moving landslides. *Vadose Zone Journal*, *10*(2), 496–511. https://doi.org/10.2136/vzj2009.0182